ASCA Observation of an "X-ray Shadow" in the Galactic Plane

Sangwook Park

Laboratory for High Energy Astrophysics, Code 662

NASA/Goddard Space Flight Center, Greenbelt, MD. 20771

and

Universities Space Research Association

Received _____; accepted _____

Submitted to the *Astrophysical Journal*

ABSTRACT

The diffuse X-ray background (DXB) emission near the Galactic plane ($l, b \sim 25.6°, 0.78°$) has been observed with *ASCA*. The observed region is toward a Galactic molecular cloud which was recently reported to cast a deep X-ray shadow in the 0.5 – 2.0 keV band DXB. The selection of this particular region is intended to provide a constraint on the spatial distribution of the DXB emission along the line of sight: i.e., the molecular cloud is optically thick at <2 keV and so the bulk of the observed soft X-rays *must* originate in the foreground of the cloud, which is at ~3 kpc from the Sun. In the 0.8 – 9.0 keV band, atomic emission lines have been detected, and the observed spectrum is primarily from thermal plasmas. Although the detailed nature of the spectrum is complicated, the observed DXB emission appears to originate from the multiple components of hot plasmas including a thermal plasma of T $\sim 10^7$ K, which prevails within ~3 kpc from the Sun.

Subject headings: diffuse radiation — Galaxy: structure — ISM: structure — X-rays: ISM

1. INTRODUCTION

The 0.1 – 0.3 keV band diffuse X-ray background (DXB) emission in the Galactic plane has been attributed to the emission from the Local Hot Bubble (LHB): a ~10^6 K plasma filling an extensive cavity, where absorbing neutral material is difficient, with an average radius of ~100 pc around the solar system (Cox & Reynolds 1987; Snowden et al. 1998). At >2 keV it has been known that there exists unresolved DXB emission along a thin disk of the plane ($-60° < l < 60°$): the so-called Galactic ridge X-ray emission (GRXE)

(Worrall et al. 1982; Warwick et al. 1985). The detection of the Fe K line emission, with a scale height of $\sim$100 pc (Yamauchi & Koyama 1993), revealed the thermal origin of the GRXE (Koyama et al. 1986a). Unresolved point sources would be insufficient to produce the observed X-ray flux (Yamauchi et al. 1997; Yamasaki et al. 1997), and the bulk of the GRXE appears to have diffuse origins such as multiple supernova remnants (Koyama et al. 1986b; Kaneda et al. 1997; Valinia & Marshall 1998). The implied temperature for the thermal plasma to make up the 2 – 10 keV GRXE ranges $\sim 10^{7.5}$ – $\sim 10^{8}$ K (Koyama et al. 1986a; Kaneda et al. 1997; Yamauchi et al. 1997; Valinia & Marshall 1998). The nature of the 0.5 – 2 keV band DXB along the plane is more elusive. The presence of a few million K Galactic gas beyond the LHB and nearby supernova remnants has been suggested in order to incorporate the observed soft X-ray emission in the plane (Nousek et al. 1982). The distribution and the spectral properties of the X-ray emitting material along the line of sight have yet to be known. One of the major advances in the study of the 0.5 – 2 keV band Galactic DXB in the plane came with the detection of "X-ray shadows" cast by distant molecular clouds. The X-ray shadows in the DXB as detected with mosaics of the *ROSAT* PSPC pointed observations in the Galactic plane have recently revealed the existence of a highly enhanced X-ray emitting region around the Galactic center: a Galactic X-ray bulge (GXB) (Park et al. 1997; Almy et al. 1998; Park et al. 1998, P98 hereafter). The derived X-ray background intensity beyond the absorbing molecular clouds is more than an order of magnitude brighter than the nominal high latitude intensity and the estimated plasma temperature of the GXB is $\sim 10^{6.6-6.7}$ K. These results are in good agreement with the *ROSAT* all-sky survey (RASS) data analysis in the general direction of the Galactic center (Snowden et al. 1997). P98 further suggested that the angular extension of the GXB along the first quadrant of the plane may be confined by the molecular ring at $l \sim 25°$. The results of these X-ray shadow studies also indicate that there exists a substantial fraction of

DXB emission originating foreground to the absorbing molecular clouds, which are located at 2 – 3 kpc from the Sun. The "foreground component" was tentatively attributed to the emission from a $\sim 10^7$ K plasma based on a band-fraction analysis (Park 1998). The extensive spectral analyses of individual DXB components along the line of sight were however infeasible with the *ROSAT* PSPC data due to the limited spectral capabilities of the PSPC mosaics.

In order for a detailed spectral study of the Galactic DXB originating foreground to the X-ray shadow clouds, an *ASCA* observation was carried out in the direction of l, $b = 25.6°$, $0.78°$. The l, $b = 25.6°$, $0.78°$ direction is toward a Galactic molecular cloud which was recently reported to cast an X-ray shadow in the 0.5 – 2.0 keV band (P98). The existence of the dense molecular cloud with a well-established distance (d $\sim$ 3 kpc) is expected to provide a useful constraint for the spatial distribution of the DXB emission along the line of sight. In other words, in the soft energy band (<2 keV), the molecular cloud is optically thick and the distance to the cloud ($\sim$3 kpc) sets a *limit* for the X-ray emitting region, or regions, along the line of sight. The contribution from unresolved stellar sources to the observed 0.5 – 2 keV band DXB in the plane has been shown to be small (Schmitt & Snowden 1990; Wang 1992; Ottmann & Schmitt 1992). *ASCA* observations of the Scutum arm region ($l \sim 28° - 29°$) have also demonstrated that only $\sim$1% of the DXB emission in the plane is from unresolved point sources (Yamauchi et al. 1997). The bulk of the DXB in the plane is therefore *truly* diffuse. The spectral study of the 0.5 – 2 keV Galactic DXB emission, the bulk of which is diffuse and originates within $\sim$3 kpc from the Sun, can thus be performed. Utilizing the full effective energy range of *ASCA*, the overall spectrum is analyzed in comparison to the previous studies of the GRXE which were performed at different directions in the sky. The observation is described in §2. The analysis and results are presented in §3 and the implications are discussed in §4. A summary and the conclusions are presented in §5.

2. OBSERVATION

The *ASCA* observation in the direction of $l, b = 25.6°, 0.78°$ was carried out on 1998 March 31 during the AO6 phase. The data from the Gas Imaging Spectrometer (GIS) were obtained in the pulse-height (PH) mode and the total exposure for each detector (GIS2 and GIS3) is ~38 ks. For the analysis the data are integrated over two detectors for the inner 30′ diameter circular region. The pointing direction ($l, b = 25.6°, 0.78°$) is centered on a Galactic molecular cloud which has an angular extent of ~1° to cast a deep X-ray shadow in the 0.5 − 2.0 keV band (P98). The exposure and vignetting corrected GIS images are displayed in Figure 1. Figure 1a is the hard band (2.0 − 9.0 keV) image and Figure 1b is the soft band (0.8 − 2.0 keV) image of the inner 30′ diameter region. The observed X-ray count rate is 0.18 ± 0.002 counts s^{-1} within 30′ diameter in the 0.8 − 9.0 keV band. In both of the soft and the hard bands, the general intensity distribution is lower around the center of the field and is higher as the angular offset from the center is larger. This overall feature of the X-ray intensity variation is reasonable considering the fact that the observation is pointed at the dense molecular cloud which cast a soft X-ray shadow. The absorbing column density of the cloud (~5.4×10^{21} cm^{-2} on average, P98) is dominant in the soft band and the more significant absorption feature is observed in the 0.8 − 2.0 keV band as displayed in Figure 1. There are a couple of faint point-like source detections within 30′ diameter in the 0.8 − 9 keV band. The source counts within 3′ radius detection circle is, however, small (~5% of the total counts).

The Solid-state Imaging Spectrometer (SIS) imposes some problems for the study of faint diffuse background emission. The SIS has experienced a decrease in detector efficiency and an increasing divergence from the GIS spectra since the early phase of the mission due to the accumulated radiation damage and the increasing fluctuation of the dark current. This degradation of the SIS performance can be substantial for the faint X-ray background

spectra and the effect is most significant in the soft band ($\lesssim$ 1 keV). The non-cosmic X-ray background subtraction for the SIS is not reliable with currently available night-Earth data and dependable spectral analysis is thus infeasible. The SIS also has a smaller effective area which also makes it inappropriate for the study of the faint diffuse background emission. The count rate for the SIS is $\sim$0.07 counts s^{-1} even with the full effective solid angle ($\sim$480 $arcmin^2$), which is only $\sim$39% of the GIS count rate of the inner 30′ diameter region. Considering that the photons detected near the edge of the nominal field of view may not be useful for the analysis, the number of utilizable photons with the SIS would be smaller than that of the GIS (30′ diameter) at least by a factor of $4 - 5$. The SIS data is therefore excluded in the spectral analysis presented in this paper although the energy resolution of the SIS is superior to that of the GIS.

3. ANALYSIS & RESULTS

3.1. Background subtraction & Energy response

As the first step of the spectral analysis the non-cosmic background is subtracted using night-Earth data. The extragalactic power law component of the DXB (presumably from unresolved AGNs) then needs to be considered since the contribution from this component in the photon energy of >2 keV is significant even in the plane. The power law component of the DXB has been extensively studied with the high latitude data and can be described with a photon index of $\Gamma \sim 1.4$ in the $2 - 10$ keV band (Gendreau 1995; Chen et al. 1997). This extragalactic power law component is included in the spectral fitting as a fixed component. In order to produce an appropriate normalization of the power law component, several high latitude "blank-sky" data are combined and fitted with a simple power law model in the $0.8 - 9$ keV band. The best fit photon index is $\Gamma = 1.46$ ($\chi^2_\nu = 1.69$) which is consistent with previous results (Ishisaki 1996). For the spectral analysis presented in the

following sections, an absorbing column density of $N_H = 4 \times 10^{22}$ cm^{-2} is assumed for the power law component accounting for the absorption by the Galactic plane. The assumed absorbing column is reasonable for the l, $b \sim 25.6°$, $0.78°$ direction considering the *low* latitude and the existence of the X-ray shadow-casting molecular cloud along the line of sight.

The study of the diffuse background emission with *ASCA* is substantially affected by the "stray light", which is a "leakage" of the photons from outside of the nominal field of view. A specific energy response of the detector must be produced to resolve this problem. For this purpose an ancillary response file (ARF) for the diffuse emission is generated by following the methods described in Kaneda et al. (1997) assuming a 1.5° radius of *uniform* diffuse emssion. (Note: Although the diffuse ARF is produced for the Galactic diffuse emission, it is also utilized in determining the normalization for the extragalactic power law component as described above. The effect is negligible for the purpose of the present work.) This specific ARF is utilized in the following spectral analysis.

3.2. Spectrum

The spectral fitting is first performed with an absorbed Raymond-Smith (RS) model assuming thermal equilibrium. The best fit plasma temperature is $kT = 6.30^{+2.58}_{-1.25}$ keV with an absorption of $N_H = 0.55^{+0.13}_{-0.14} \times 10^{22}$ cm^{-2} (the errors refer to a 90% confidence level, hereafter). The best fit model is displayed in Figure 2. In Figure 2 the fixed extragalactic power law component is represented with a dashed line and the contribution is shown to be limited to $E > 2$ keV due to the absorption by the plane. Although the overall fit is statistically good ($\chi^2_\nu = 0.98$), it is clearly observed that the data are in good agreement with the model only at >2 keV (Figure 2). The fit is unacceptable ($\chi^2_\nu = 3.63$) at <2 keV and the DXB of this energy was the motivation of the present work. It is however

interesting to note that the best fit parameters may at large represent the GRXE spectrum of $kT = \sim 6$ keV as absorbed by the molecular cloud ($N_H \sim 5.4 \times 10^{21}$ cm^{-2} on average) that casts the 0.5 – 2.0 keV X-ray shadow.

A second RS component is then added in the model. The best fit parameters are summarized in Table 1 and the fit is displayed in Figure 3 (Model 1 hereafter). The fit is good even at <2 keV ($\chi^2_\nu = 0.92$) and the overall statistics also improved ($\chi^2_\nu = 0.59$). The soft component ($kT = 0.64$ keV) makes up most (~75%) of the 0.5 – 2.0 keV band emission and the contribution from this component to the 2 – 10 keV band count rate is small (~6%). Since the molecular cloud is opaque at <2 keV and so casts a deep X-ray shadow in the 0.5 – 2.0 keV band DXB, the bulk of the soft component *must* originate in the foreground of the cloud. The implied absorbing column ($N_H = 1.21 \times 10^{22}$ cm^{-2}), however, indicates a distance of $\gtrsim$3 kpc to the emission region assuming an average space density of 1 cm^{-3} in the plane. This distance scale locates the emitting region "behind" of the molecular cloud, which is inconsistent with a foreground (to the cloud) origin for the soft component. The 1.5 keV band (0.73 – 2.04 keV, corresponding to the R6 + R7 band for the *ROSAT* PSPC) to 3/4 keV band (0.44 – 1.21 keV, corresponding to the R4 + R5 band for the *ROSAT* PSPC) (Snowden et al. 1994) hardness ratio of the count rates for the modeled spectrum is 2.4. This hardness ratio is harder than the observed value of the foreground count rates of the X-ray shadow in the same region as detected with *ROSAT* (1.4, P98). The large hardness ratio and absorbing column for the modeled soft component are further discussed in §4.1

After deabsorbing the spectrum, the estimated model flux for the soft component is 6.08×10^{-10} ergs s^{-1} cm^{-2} in the 0.5 – 2.0 keV band. Assuming an effective solid angle of 1.5° radius, the surface brightness can be estimated to be 2.8×10^{-7} ergs s^{-1} cm^{-2} sr^{-1}. Since the distribution of the X-ray emitting plasma is unclear along the line of sight, a

reasonable range of 1 – 3 kpc is assumed for the depth of the emitting region. The volume emissivity then ranges 0.38 – 1.14 × 10^{-27} ergs s^{-1} cm^{-3} in the 0.5 – 2.0 keV band. The total luminosity is 2.1 – 6.3 × 10^{37} ergs s^{-1} assuming a disk-like emission region with a thickness of 200 pc. Since ~98% of the model flux is produced in the 0.5 – 2.0 keV band for the soft component, these values are almost identical for the 0.5 – 10.0 keV band. The plasma parameters are summarized in Table 2.

The hard component (kT = 3.7 keV) dominates the observed spectrum at >2 keV and produces ~68% of the count rates in the 2 – 10 keV band. The implied foreground column, N_H = ~2.5 × 10^{22} cm^{-2}, indicates that this component originates beyond the molecular cloud. The hard component is also responsible for the Fe line emission at ~6.7 keV (Figure 3). After removing the absorption, the estimated model flux for the hard component is 4.23 × 10^{-10} ergs s^{-1} cm^{-2} in the 0.5 – 10.0 keV band and the surface brightness is 2.0 × 10^{-7} ergs s^{-1} cm^{-2} sr^{-1}. Assuming ~15 kpc for the depth of the emitting region along the line of sight, the volume emissivity can be estimated to be ~0.53 × 10^{-28} ergs s^{-1} cm^{-3}. For the emission volume of ~1.8 × 10^{66} cm^3 (assuming a thin disk with a radius of 10 kpc and a thickness of 200 pc), the total luminosity is estimated to be ~1.0 × 10^{38} ergs s^{-1}. The plasma parameters are summarized in Table 2.

3.3. Atomic Line Emission

The observed spectrum exhibits atomic emission lines which support the thermal origin of the DXB. First of all, the Fe K line at ~6.7 keV is clearly observed (Figure 3). In the 3 – 9 keV band, the spectrum can be fitted with a thermal bremsstrahlung and a Gaussian line in order to determine the center energy of the Fe K line. The best fit line energy is $6.62^{+0.13}_{-0.14}$ keV where the continuum temperature is $kT = 3.67^{+4.16}_{-1.67}$ keV with an absorption of N_H ~ 2.1 × 10^{22} cm^{-2} ($\chi^2_\nu = 0.45$). The line width was fixed at zero assuming a narrow emission

line. When the line width is allowed to vary the best fit value is 233 eV with the uncertainty covering zero, which makes the narrow line assumption reasonable. After determining the continuum temperature of the hard component and the Fe K line energy, the line energies and plasma temperature for the soft band emission are fitted. Since there seem to exist at least a couple of emission lines at $\sim$1.8 keV and $\sim$1.3 keV (Figure 3), with the best fit hard component parameters fixed as determined above, another bremsstrahlung model with two Gaussian components are added in the $0.8 - 9$ keV band. Despite the large uncertainty, the absorbing column for the hard component is fixed at the best fit value (2.1×10^{22} cm^{-2}) since it is consistent with the Galactic absorption by the plane as well as the result of the two component RS model (Model 1) as presented in §3.2. The best fit line energies are then $1.84^{+0.10}_{-0.07}$ keV and $1.21^{+0.05}_{-0.07}$ keV. The best fit continuum temperature is $kT = 1.02^{+8.79}_{-0.71}$ keV with a low absorption of $N_H = 0.07 \times 10^{22}$ cm^{-2}. The uncertainty for the absorption covers zero and a 2σ upper limit is 1.17×10^{22} cm^{-2}. The line widths are again set to zero assuming narrow lines, as well as to help constrain the other fitted parameters. The overall fit is good with $\chi^2_\nu = 0.45$. The best fit model (Model 2 hereafter) is displayed in Figure 4 and the model paramters are presented in Table 3. The 1.84 keV line is identified with the Si K line. The identification of the 1.21 keV line is unclear and may represent a blend of unresolved lines such as Mg K (1.35 keV) and Fe L (1.08 keV) lines as detected by Kaneda et al. (1997) toward the Scutum arm region. Unfortunately, the quality of the current data is insufficient for further investigations of this "1.21 keV line" feature (Note: While not being utilized in the present work, a preliminary SIS spectrum was generated in order to entertain the possibility for the detection of any unresolved lines between 1 keV and 2 keV. An indication of the Fe L line is observed, but the evidence is weak with no statistical significance due to the low quality of the data). The best fit plasma temperature ($kT = 1.02$ keV) for the soft component is higher than Model 1 ($kT = 0.64$ keV) while the absorption becomes negligible. The low absorption is in good agreement with the assumption of the

foreground (to the cloud) origin of the soft component. The 1.5 keV to 3/4 keV hardness ratio of the count rates is 1.2, which is also consistent with the *ROSAT* result. With the Gaussian line components, the soft component makes up 67% of the total count rate in the 0.5 – 2.0 keV band. After deabsorbing the spectrum, the 0.5 – 2.0 keV band flux for the soft component is 4.57×10^{-11} ergs s^{-1} cm^{-2}. The surface brightness is 0.21×10^{-7} ergs s^{-1} cm^{-2} sr^{-1}. Assuming a range of 1 – 3 kpc of the emitting region along the line of sight, the volume emissivity is $0.29 - 0.87 \times 10^{-28}$ ergs s^{-1} cm^{-3}. The total luminosity is $1.6 - 4.8 \times 10^{36}$ ergs s^{-1} assuming a disk-like emission region with thickness of 200 pc. Since the bulk (~85%) of the model flux from this component is produced in the 0.5 – 2.0 keV band, the modeled plasma parameters are compatible in the 0.5 – 10.0 keV band as summarized in Table 4. The best fit parameters for the hard continuum (kT = ~3.7 keV, N_H = ~2.1 $\times$ 10^{22} cm^{-2}) are almost identical to those of Model 1. After removing the absorption, the estimated plasma parameters for the hard component are summarized in Table 4.

4. DISCUSSION

4.1. The Soft Component

The best fit plasma temperature for the soft component is kT = ~0.6 keV (Model 1) – ~1.0 keV (Model 2), which is higher than that of the GXB (kT = 0.35 keV) (Snowden et al. 1997). Park (1998) has suggested that the foreground DXB emission (originating at $\lesssim$3 kpc) of the 0.5 – 2 keV band X-ray shadows in the l, b = 10°, 0° and l, b = 25°, 0.5° directions may arise from a $kT \sim$ 0.9 keV plasma. Kaneda et al. (1997) demonstrated that the soft component of the GRXE toward the Scutum arm region (l = 28° – 29°) has a temperature of kT = 0.8 keV. The present results are in good agreement with these previous works. The implied absorption is however controversial between Model 1 and Model 2. The absorbing column for Model 1 is fairly large (~1.2×10^{22} cm^{-2}) indicating

the emitting region is at $\gtrsim$3 kpc. On the other hand the best fit absorbing column for Model 2 is small ($\sim 0.1 \times 10^{22}$ cm^{-2}) with a 2σ upper limit of $\sim 1.2 \times 10^{22}$ cm^{-2}. Model 2 implies that the soft component has a nearby origin, most likely within $\sim$1 kpc. Due to the opacity of the absorbing molecular cloud, the soft component can safely be assumed to be responsible for the Galactic DXB emission which originates in the foreground of the cloud. The implied distance scale to the emitting region in Model 1 is thus inconsistent with this assumption whereas Model 2 is in good agreement. It is also noticed that the 1.5 to 3/4 keV hardness ratio of the count rates in Model 1 (2.4) is inconsistent with the *ROSAT* data (1.4, P98) while Model 2 hardness ratio (1.2) is close to the *ROSAT* result. The implied far distance scale to the emitting region and the large hardness ratio for Model 1 suggest that the absorbing column in Model 1 might be overestimated. Although the origin of the disagreements in Model 1 is unclear, the confusion might be caused by the relatively low quality of the current data. The sensitivity and energy resolution of the GIS decrease significantly at $\lesssim$1 keV and the current data appear insufficient to resolve the emission lines at <2 keV with Model 1. In Model 1 the residuals display a systematic deviation from the best fit model at $E < 2$ keV, which suggests that the best fit soft RS component might be biased due to the presence of the unresolved lines. In Model 2, with separate Gaussian components for the possible lines, the fit improves in the low energy band. Although simple Gaussians may not be adequate to represent the lines in this case as demonstrated with the unidentified "1.2 keV line" in Model 2, the overall feature appears to be better described with the separate Gaussian components. The plasma may also be in a non-equilibrium (Kaneda et al. 1997) causing the descrepancies. Follow up observations with better statistics and/or a better spectral resolution will be helpful to resolve the origin of the imposed discrepancies.

The 0.5 – 10 keV band surface brightness in both of Model 1 (2.9×10^{-7} ergs s^{-1} cm^{-2} sr^{-1}) and Model 2 (0.3×10^{-7} ergs s^{-1} cm^{-2} sr^{-1}) of the unabsorbed soft component

is substantially lower than the previous result at $b = 0°$ ($\sim 1.9 \times 10^{-6}$ ergs s^{-1} cm^{-2} sr^{-1}) (Kaneda et al. 1997). The lower surface brightness may be in part related to the embedded inaccuracy in the model fittings as described above. It may also be due to the "higher" latitude of the current data (centered on $b = \sim 0.8°$) since the DXB near the plane has a significant flux variations along the latitudes (Kaneda et al. 1997). With the estimated volume emissivity the mean electron density of the plasma can be calculated by the relation, $\epsilon = n_e^2 \Lambda(\mathrm{T})$, where ϵ is the emissivity, and n_e is the electron density. The cooling function $\Lambda(\mathrm{T})$ is estimated to be,

$$\Lambda(T) \; = \; 6.2 \times 10^{-19} \, T^{-0.6}, \; 0.009 \; keV < kT < 3.4 \; keV$$

$$\Lambda(T) \; = \; 2.5 \times 10^{-27} \, T^{0.5}, \; kT > 3.4 \; keV$$

(McKee & Cowie 1977). Depending on the emission volumes, the estimated electron density ranges $0.003 - 0.005$ cm^{-3} for Model 1 and $0.001 - 0.002$ cm^{-3} for Model 2. The thermal pressure (p/k) can then be estimated as $p/k = 3 n_e \mathrm{T}$ assuming the adiabatic phase of the plasma. The derived p/k ranges $6.5 - 11.1 \times 10^4$ K cm^{-3} for Model 1 and $1.8 - 3.3 \times 10^4$ K cm^{-3} for Model 2.

4.2. The Hard Component

A hard component with $kT = 5 - 10$ keV has been reported for the GRXE (Koyama et al. 1986a; Kaneda et al. 1997; Yamauchi et al. 1997). The GRXE as observed with *RXTE* is however suggested to arise from a $\sim 2 - 3$ keV plasma as well as from a power law component of $\Gamma \sim 1.8$ which dominates at >10 keV (Valinia & Marshall 1998). Valinia & Marshall (1998) attributed the difference among the plasma temperatures of the GRXE hard component to a different interpretation of the "additional" power law component as observed with *RXTE*. As for the previous works, an "effective" temperature range of $kT =$

$5 - 10$ keV is therfore assumed for the hard component GRXE in the following discussion. The present result implies that the hard component of the Galactic X-ray background in the plane is from a $kT = \sim 4$ keV plasma. Although the additional power law component as indicated by Valinia & Marshall (1998) was not included in the current work, the best fit hard component temperature still appears to be lower than $5 - 10$ keV. The $kT = \sim 4$ keV is persistent in both Model 1 and Model 2. While the origin of the "lower" plasma temperature component is unclear, it might be due to the complicated Galactic structure in the $l \sim 25°$ direction. The $l \sim 25°$ direction of the plane has been suggested to be a "transition" region between the GXB and the molecular ring (P98). The angular extension of the molecular ring ($-60° < l < 60°$) (Dame et al. 1987) is coincident with that of the GRXE. The molecular ring may trace the active star-forming regions in the Galaxy and be spatially correlated with the emitting regions of the GRXE as suggested by Yamauchi & Koyama (1993). The estimated temperature of the GXB plasma is most likely $kT =$ 0.35 keV (Snowden et al. 1997; Park 1998). Assuming that the $l \sim 25°$ direction beyond the absorbing cloud is a transition region between the GXB and the hard component GRXE, the relatively lower temperature of the present data may reflect the existence of the "cooler" GXB plasma along the line of sight. Observations at various longitudes along the plane are needed to test this speculation. The disagreement may also be purely due to the relatively poor quality of the data since the statistical uncertainties in the model fittings of the present work are generally large. Follow-up observations with upcoming missions such as *XMM* will be helpful to resolve the confusions in this work.

Assuming that the hard component occupies a thin disk along the plane (with a thickness of $\sim$ 200 pc, and a radius of $\sim$ 10 kpc), the total luminosity is $\sim 1.0 \times 10^{38}$ ergs s^{-1}. This total luminosity is in good agreement with the previous results for the hard component GRXE ($\sim 1 - 2 \times 10^{38}$ ergs s^{-1}) (Worrall et al. 1982; Koyama et al. 1986a; Kaneda et al. 1997; Valinia & Marshall 1998). The estimated electron density is $\sim$0.002

cm^{-3} and the thermal pressure is $p/k = 2.3 \times 10^5$ K cm^{-3}.

5. SUMMARY AND CONCLUSIONS

The Galactic X-ray background emission in the direction of $l,\ b = 25.6°,\ 0.78°$ is observed with *ASCA*. The observed pointing direction is toward a dense molecular cloud which casts an X-ray shadow in the $0.5 - 2$ keV band. The kinematic distance to the cloud ($\sim$3 kpc) together with the detected shadowing feature makes it possible to study the spectral properties of the Galactic X-ray background emission originating in the foreground of the Galactic X-ray bulge yet beyond the Local Hot Bubble. The observed spectrum can be fitted with a two component thermal plasma model. The soft component is most likely from a $kT = 0.64$ keV Raymond-Smith plasma and dominates the observed spectrum at <2 keV. The implied foreground column density and the hardness ratio are however large and inconsistent with the *ROSAT* data. The hard component is from a $kT = \sim 4$ keV plasma and absorbed by the Galactic plane. The best fit temperature is however lower in comparison to the previous studies of the GRXE. When the detected atomic emission lines are separately fitted with narrow Gaussian profiles, the soft component cotinuum is best fitted with $kT = \sim 1$ keV with limited absorption. The implied distance scale to the bulk of the emission region (most likely $\lesssim 1$ kpc) and the hardness ratio are consistent with the *ROSAT* data. The hard component fitting for the continuum with the separate Gaussian lines results in little change implying the existence of a $kT = \sim 4$ keV thermal plasma across the Galactic plane.

The present results confirm that the multi-component thermal plasmas are responsible for the observed Galactic X-ray background in the plane. Although the conflicts regarding the details of the individual components may be in part due to the complicated Galactic structure in the plane, the relatively low quality of the current data may also be responsible.

Follow up observations of the Galactic DXB for various directions along the plane with upcoming missions such as *XMM* will be necessary to resolve the controversies imposed in this work and to unravel the Galactic DXB structure.

The author thank S. Snowden for the constructive discussion, and A. Valinia for valuable comments at the early stage of this work. The author gives a special thank to K. Ebisawa for his help in generating the diffuse ARF and the "blank-sky" data utilized in this study. This work was supported by USRA and NASA Cooperative Agreement NCC 5-356.

REFERENCES

Almy, R. C., McCammon, D., Digel, S. W., Bronfman, L., & May, J. 1998, ApJ, Submitted

Cox, D. P. & Reynolds, R. J. 1987, ARA&A, 25, 303

Chen, L.-W, Fabian, A.C., & Gendreau, K. C. 1997, MNRAS, 285, 449

Dame, T. M., Ungerechts, H., Cohen, R.S., de Geus, E. J., Grenier, I. A., May, J., Murphy, D. C., Nyman, L. -Å, & Thaddeus, P. 1987, ApJ, 322, 706

Gendreau, K. C. 1995, Ph.D. Thesis, Massachusetts Institute of Technology

Ishisaki, Y. 1996, Ph.D. Thesis, University of Tokyo

Kaneda, H., Makishima, K., Yamauchi, S. Koyama, K., Matsuzaki, K, & Yamasaki, N. Y. 1997, ApJ, 491, 638

Koyama, K., Makishima, K., Tanaka, Y., & Tsunemi, H. 1986a, PASJ, 38, 121

Koyama, K., Ikeuchi, S., & Tomisaka, K. 1986b, PASJ, 38, 503

McKee, C. F., & Cowie, L. L. 1977, ApJ, 215, 213

Nousek, J. A., Fried, P. M., Sanders, W. T., & Kraushaar, W. L. 1982, ApJ, 258, 83

Ottmann, R., & Schmitt, J. H. M. M. 1992, A&A, 256, 421

Park, S., Finley, J. P., Snowden, S. L., & Dame, T. M. 1997, ApJ, 476L, L77

Park, S. 1998, Ph.D. Thesis, Purdue University

Park, S., Finley, J. P., & Dame, T. M. 1998, ApJ, 509, 203 (P98)

Schmitt, J. H. M. M. & Snowden, S. L. 1990, ApJ, 361, 207

Smith, R., 1999, private communications

Snowden, S. L., McCammon, D., Burrows, D. N., & Mendenhall, J. A. 1994, ApJ, 424, 714

Snowden, S. L., Egger, R., Freyberg, M. J., McCammon, D., Plucinsky, P. P., Sanders, W. T., Schmitt, J. H. M. M., Trümper, J., & Voges, W., 1997, ApJ, 485, 125

Snowden, S. L., Egger, R., Finkbeiner, D. P., Freyberg, M. J., & Plucinsky, P. P. 1998, ApJ, 493, 715

Valinia, A., & Marshall, F. E. 1998, ApJ, 505, 134

Wang, Q. D. 1992, ApJ, 392, 509

Warwick, R. S., Turner, M. J. L., Watson, M. G., & Willingale, R. 1985, Nature, 317, 218

Worrall, D. M., Marshall, F. E., Boldt, E. A., & Swank, J. H. 1982, ApJ, 255, 111

Yamasaki, N. Y., Ohashi, T., Takahara, F., Yamauchi, S., Koyama, K., Kamae, T., Kaneda, H., Makishima, K., Sekimoto, Y., Hirayama, M., Takahashi, T., Yamagami, T., Gunji, S., Tamura, T., Miyazaki, S., & Nomachi, M. 1997, ApJ, 481, 821

Yamauchi, S., & Koyama, K. 1993, ApJ, 404, 620

Yamauchi, S., Kaneda, H., Koyama, K., Makishima, K., Matsuzaki, K, Sonobe, T., Tanaka, Y., & Yamasaki, N. Y. 1997, *X-ray Imaging and Spectroscopy of Cosmic Hot Plasmas* Proceedings of International Symposium on X-ray Astronomy, edited by F. Makino & K. Mitsuda, (Universal Academy Press, Inc. Tokyo, Japan), 145

This manuscript was prepared with the AAS LaTeX macros v5.0.

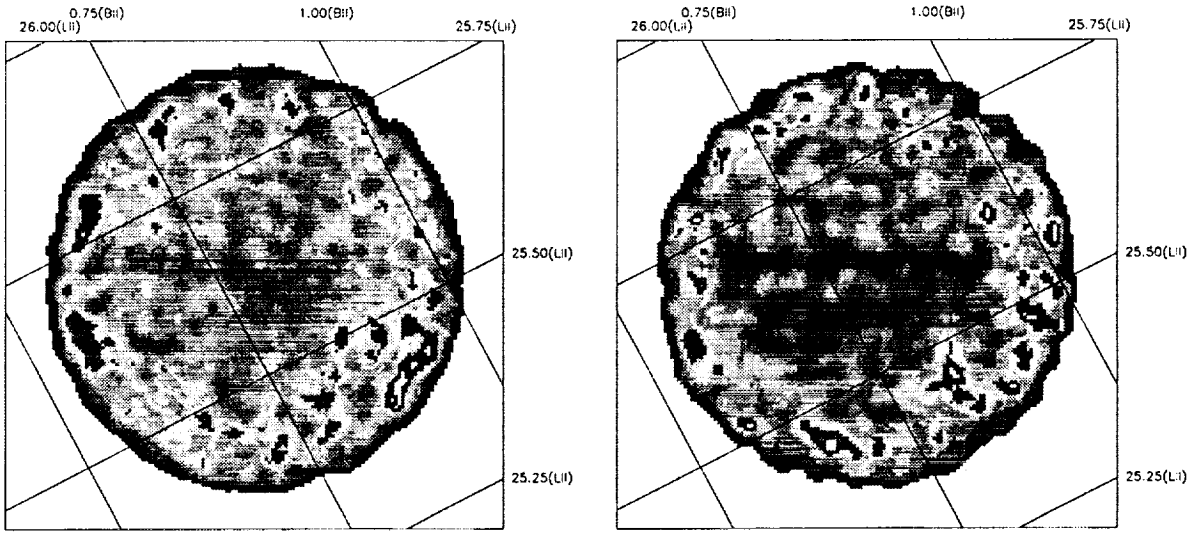

Fig. 1.— *Left*: (a) The exposure and vignetting corrected 2.0 – 9.0 keV band *ASCA* (GIS2+GIS3) image. *Right*: (b) The exposure and vignetting corrected 0.8 – 2.0 keV band *ASCA* (GIS2+GIS3) image. Both images are smoothed with a Gaussian with σ=2 pixels.

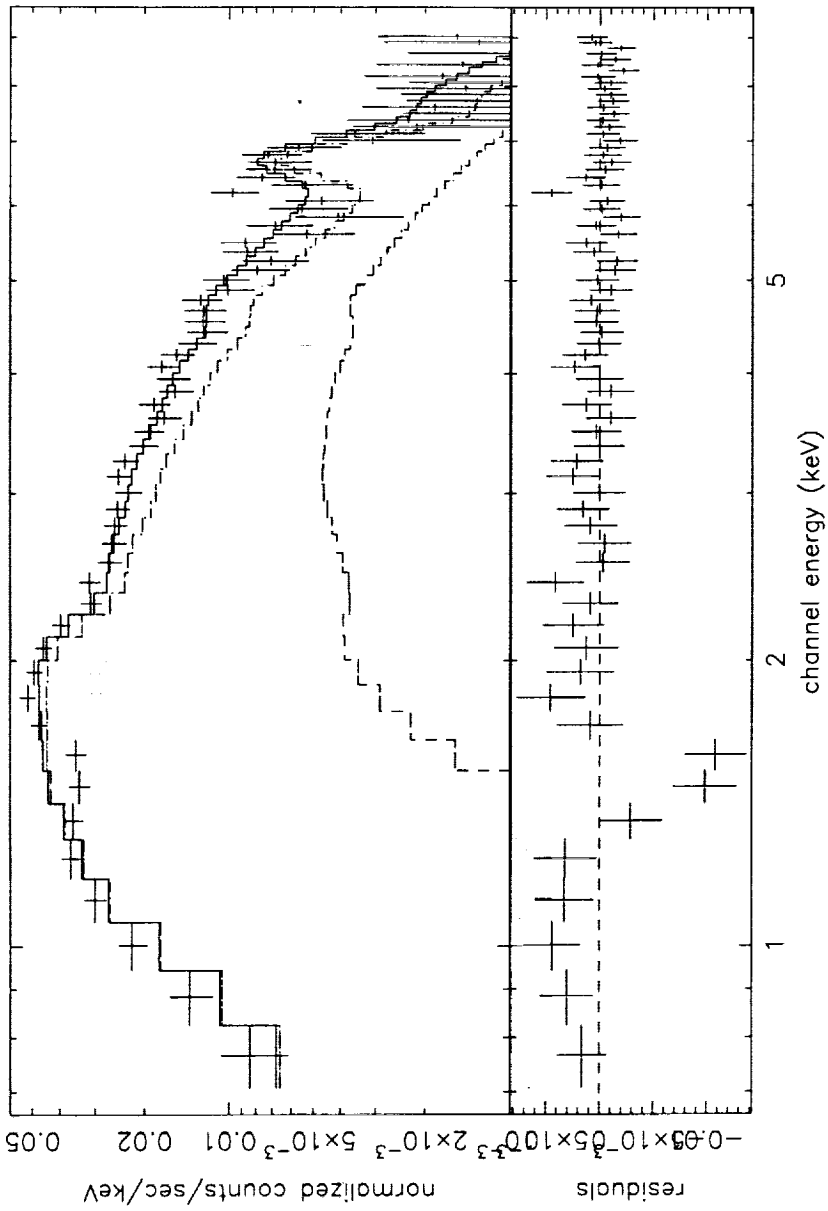

Fig. 2.— The ASCA/GIS spectrum folded through the instrumental response with the best-fit one component Raymond-Smith model. The dashed line represents the fixed extragalactic power law component and the dot-dashed line is the fitted Raymond-Smith component.

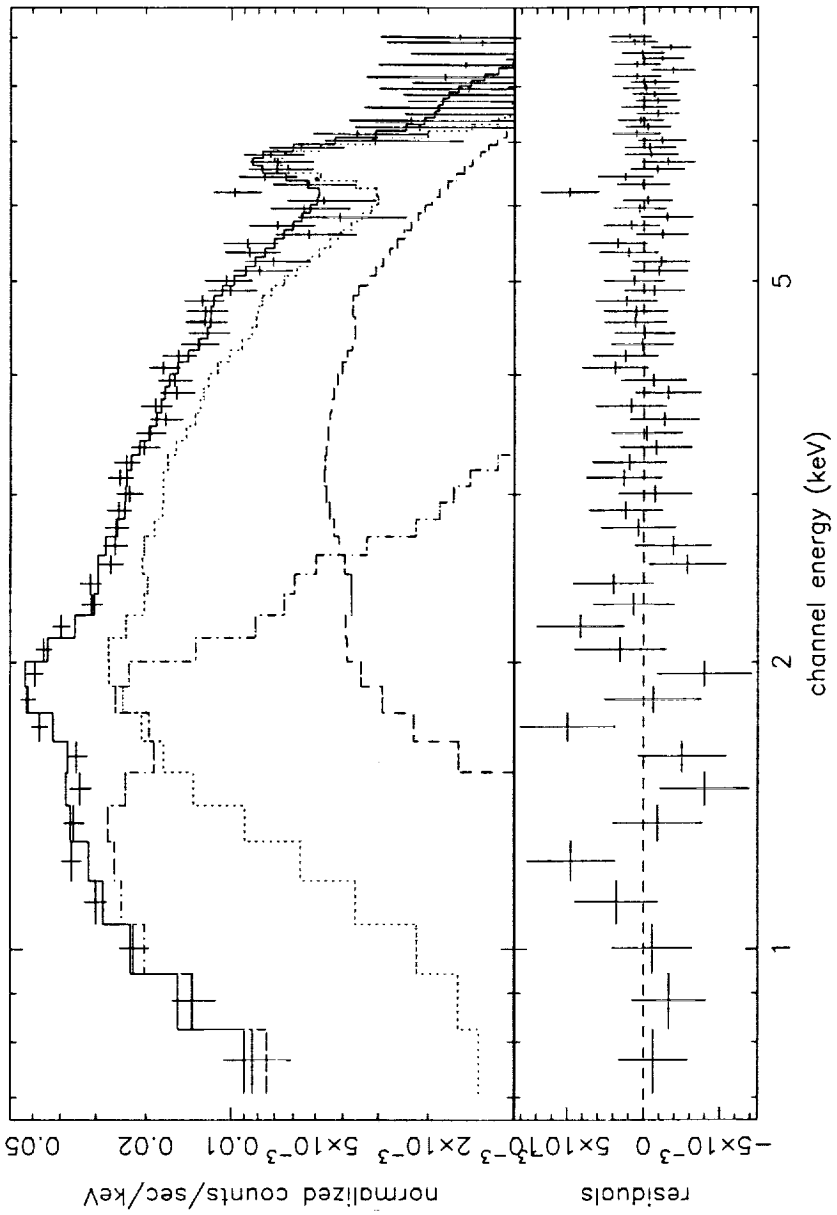

Fig. 3.— The ASCA/GIS spectrum folded through the instrumental response with the best-fit two component Raymond-Smith model. The dashed line is the fixed extragalactic power law. The dot-dashed line represents the best fit soft component of the Raymond-Smith and the dotted line is the best fit hard component of the Raymond-Smith model.

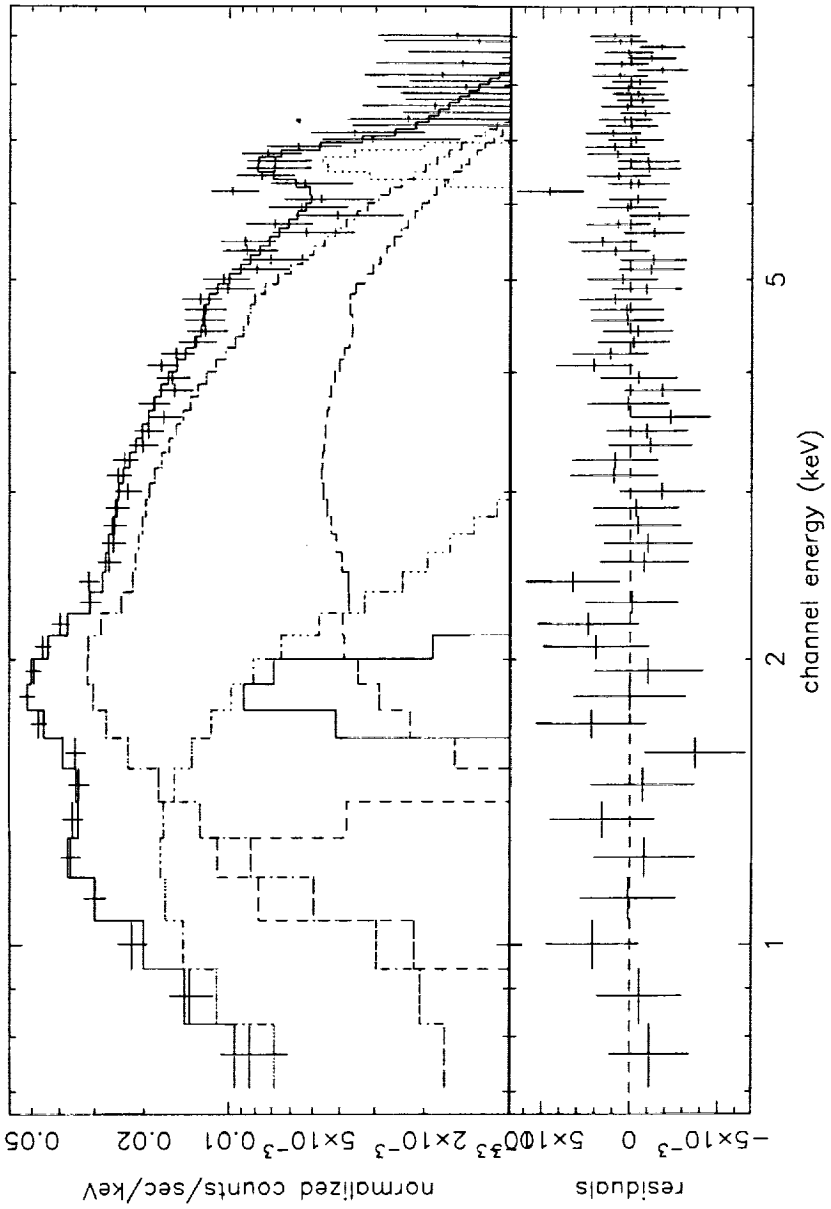

Fig. 4.— The ASCA/GIS spectrum folded through the instrumental response with the best-fit two component thermal bremsstrahlung + narrow Gaussians. The dashed line is the fixed extragalactic power law component. The dot-dashed line is the best fit hard component of the continuum and the dot-dot-dashed line is the best fit soft continuum. The three narrow Gaussian profiles for the atomic emission lines are also displayed at 1.21 keV, 1.84 keV, and 6.62 keV, respectively.

Table 1. Best fit parameters for two component Raymond-Smith model (Model 1).

	N_H (10^{22} cm^{-2})	kT (keV)
Soft	$1.21^{+0.23}_{-0.29}$	$0.64^{+0.13}_{-0.16}$
Hard	$2.47^{+1.13}_{-0.94}$	$3.71^{+1.50}_{-0.79}$
χ^2_ν=0.59		

Table 2. Summary of plasma parameters (0.5 – 10.0 keV) for the two-temperature Raymond-Smith model (Model 1) after removing the absorption.

Parameter	Soft	Hard
Flux (ergs s^{-1} cm^{-2})	6.22×10^{-10}	4.23×10^{-10}
Surface Brightness (ergs s^{-1} cm^{-2} sr^{-1})	2.9×10^{-7}	2.0×10^{-7}
Volume Emissivity (ergs s^{-1} cm^{-3})	$0.39 - 1.18 \times 10^{-27}$	0.53×10^{-28}
Total Luminosity (ergs s^{-1})	$2.2 - 6.5 \times 10^{37}$	1.0×10^{38}
Electron Density (cm^{-3})	0.003 – 0.005	0.002
Thermal Pressure (p/k, K cm^{-3})	$6.5 - 11.1 \times 10^{4}$	2.3×10^{5}

Table 3. Best fit parameters for bremsstrahlung + Gaussian model (Model 2).

	N_H (10^{22} cm^{-2})	kT (keV)
Soft	<1.17[a](0.07)	$1.02^{+8.79}_{-0.71}$
Hard	2.1[b]	3.67[b]
χ^2_ν=0.45		

[a]This is a 2σ upper limit. The number in the parenthesis is the best fit value.

[b]This is the best fit value from the hard component fit in the 3 – 9 keV band and is fixed in the fitting.

Table 4. Summary of plasma parameters (0.5 – 10.0 keV) for the bremsstrahlung + Gaussian model (Model 2) after removing the absorption.

Parameter	Soft	Hard
Flux (ergs s^{-1} cm^{-2})	5.38×10^{-11}	4.18×10^{-10}
Surface Brightness (ergs s^{-1} cm^{-2} sr^{-1})	0.25×10^{-7}	1.94×10^{-7}
Volume Emissivity (ergs s^{-1} cm^{-3})	$0.34 - 1.02 \times 10^{-28}$	0.53×10^{-28}
Total Luminosity (ergs s^{-1})	$0.2 - 0.6 \times 10^{37}$	1.0×10^{38}
Electron Density (cm^{-3})	0.001 – 0.002	0.002
Thermal Pressure (p/k, K cm^{-3})	$1.8 - 3.3 \times 10^{4}$	2.3×10^{5}